Materials Letters 233 (2018) 158–161

Contents lists available at ScienceDirect

Materials Letters

journal homepage: www.elsevier.com/locate/mlblue

Carbon-coated CoS@rGO anode material with enhanced cyclic stability for sodium storage

Hao Jia [a,b], Mahmut Dirican [b,*], Chen Chen [b], Pei Zhu [b], Chaoyi Yan [b], Xia Dong [b], Zhuang Du [b], Jiansheng Guo [a], Jiasheng Wang [c], Fangcheng Tang [c], Jinsong Tao [d,*], Xiangwu Zhang [b,*]

[a] Key Laboratory of Textile Science and Technology, Ministry of Education, College of Textiles, Donghua University, Shanghai 201620, China
[b] Fiber and Polymer Science Program, Department of Textile Engineering, Chemistry and Science, College of Textiles, North Carolina State University, Raleigh, NC 27695-8301, USA
[c] Guangzhou Lushan New Materials Co., Ltd., Guangzhou 510530, China
[d] State Key Laboratory of Pulp and Paper Engineering, South China University of Technology, Guangzhou 510640, China

ARTICLE INFO

Article history:
Received 27 July 2018
Received in revised form 14 August 2018
Accepted 29 August 2018
Available online 30 August 2018

Keywords:
Cobalt sulfide
Sodium-ion batteries
Carbon coating
High cycling stability

ABSTRACT

Carbon-coated cobalt sulfide@reduced graphene oxide (CoS@rGO@C) composite was innovatively synthesized by a simple solvothermal reaction and subsequent carbon coating process for use as the anode material in sodium-ion batteries (SIBs). In this composite structure, the rGO network and extra outer carbon coating worked synergically to achieve excellent electrode architecture stability upon long-term cycling. Specifically, the CoS@rGO@C composite anode demonstrated superior reversible capacity (706 $mAh{\cdot}g^{-1}$ at 100 $mA{\cdot}g^{-1}$ at the 1st cycle), high rate capability (374 $mAh{\cdot}g^{-1}$ at 1.6 $A{\cdot}g^{-1}$), and remarkably stable cycling performance (80% capacity preservation for up to 100 cycles) based on the synergistic action of rGO and carbon coating on CoS. In addition to improving the electrochemical performance of CoS anodes, this composite material strategy can be conveniently adapted to other metal-based anode designs to improve their cycling stability and promote their application in energy storage.

1. Introduction

Sodium-ion batteries (SIBs) gradually become attractive substitute to lithium-ion batteries for stationary energy storage equipment mainly due to the natural abundance and low price of sodium [1]. Currently, advanced electrode materials for SIBs are highly requested to overcome their present general deficiencies, such as low energy density and unstable cycling performance [2,3]. Among various anode candidates for SIBs, metal sulfides are one of the most appropriate anode materials owing to their compatible reaction potential for Na-ion storage and relatively low volumetric variation during the cycling [4].

Compared to other metal sulfides, cobalt sulfides attract more attention as a host material for sodium ions because of their considerable reversible capacity, acceptable price, and eco-environmental feature. Zhou et al. introduced Co_3S_4 nanosheets inserted in flexible graphene sheets as an anode material for SIB, which presented a charge capacity of 329 $mAh{\cdot}g^{-1}$ at 0.5 $A{\cdot}g^{-1}$ and retained 71% of its initial capacity after 50 cycles [5]. Additionally, Shao et al. synthesized a CoS_2@reduced graphene oxide (rGO) hybrid anode by one-step hydrothermal route and this CoS_2/rGO composite anode exhibited a high original specific capacity of 750 $mAh{\cdot}g^{-1}$ at 100 $mA{\cdot}g^{-1}$ while the capacity decreased to 400 $mAh{\cdot}g^{-1}$ after 100 cycles [6]. Therefore, for achieving high capacity and satisfactory cycle stability in cobalt sulfide-based anodes, novel structure designs need to be introduced for accommodating the severe volume changes of cobalt sulfides during cycling.

In this study, we rationally designed an integrated anode material of CoS@rGO@C for SIBs by an efficient hydrothermal reaction and subsequent carbon coating process (Fig. 1). Impressively, our results demonstrated the rGO network and extra outer carbon coating could work synergically to effectively buffer the volume variation of the active material (CoS) during repeated cycling. In addition, the electronically conductive carbon structure can boost the efficient electron transfer, which accelerates the electrode kinetics and reduces the electrolyte resistance.

2. Results and discussion

The morphologies of CoS@rGO and CoS@rGO@C are first detected by SEM images (Fig. 2a and b). It is observed that the rGO sheets in CoS@rGO presented obvious stratified structure with

* Corresponding authors.
E-mail addresses: mdirica@ncsu.edu (M. Dirican), jstao@scut.edu.cn (J. Tao), xiangwu_zhang@ncsu.edu (X. Zhang).

https://doi.org/10.1016/j.matlet.2018.08.150
0167-577X/

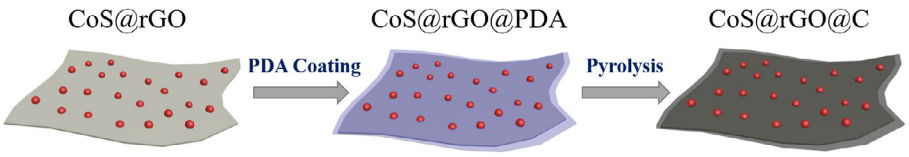

Fig. 1. Illustration of the fabrication procedures of CoS@rGO@C.

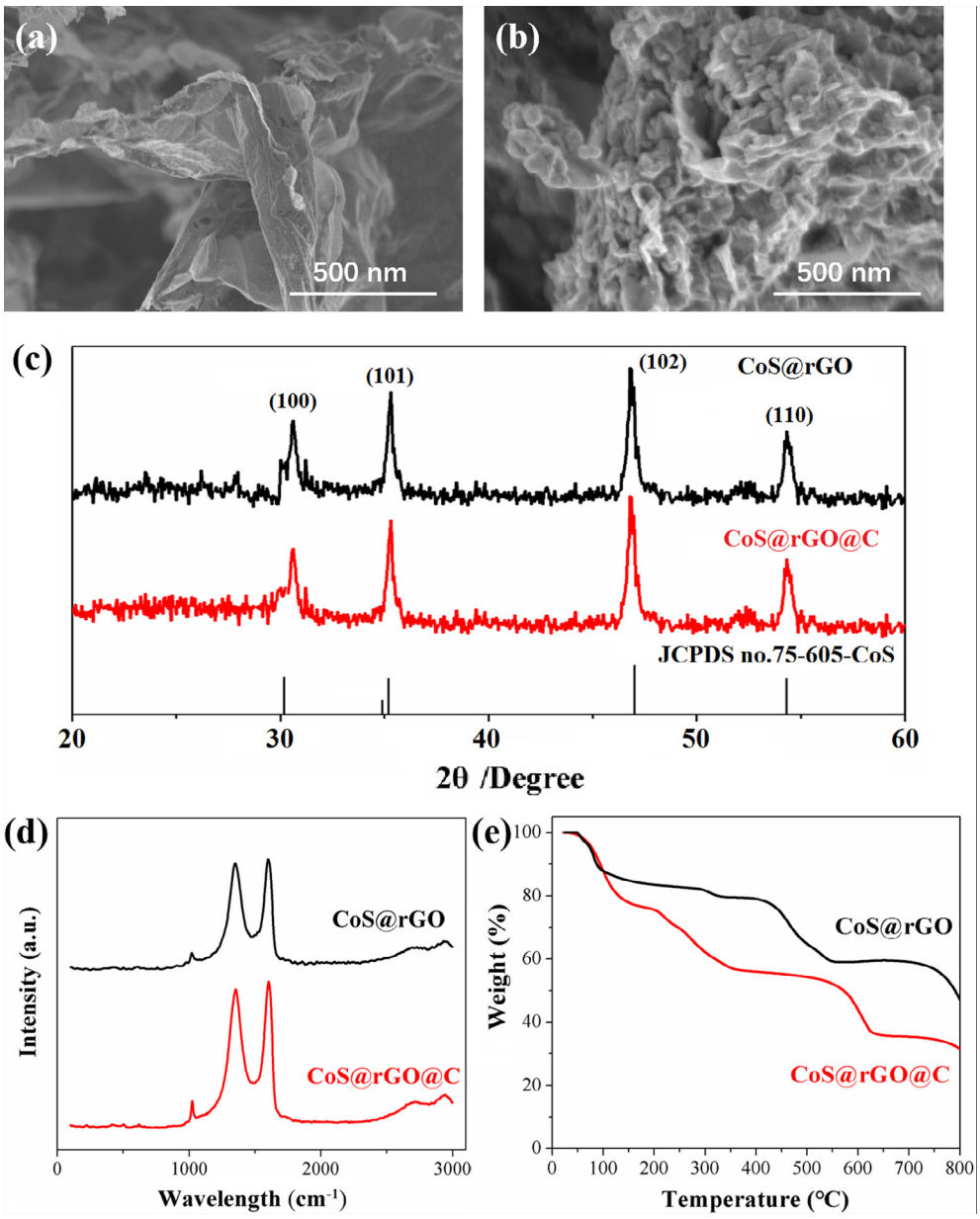

Fig. 2. SEM images of CoS@rGO (a) and CoS@rGO@C (b). XRD patterns (c), Raman spectra (c) and TGA (d) of CoS@rGO and CoS@rGO@C.

some wrinkles and the CoS particles were anchored onto the rGO sheets densely and uniformly (Fig. 2a). After carbon coating, CoS@rGO@C retained the stratified structure of rGO sheets integrally (Fig. 2b). It is noteworthy to mention that this consecutive conductive rGO network would help improve the electron conduction property of the electrode while the outer carbon coating would further enhance the electrode structure stability to endure the detrimental volume variation during repeated charge-discharge processes.

Fig. 2c depicts the XRD patterns of CoS@rGO and CoS@rGO@C. Diffraction peaks detected at $2\theta = 30.2°$, 35.2°, 47° and 54.3° could be indexed to the hexagonal CoS. Furthermore, no characteristic diffraction peak of graphene at 24.5° or carbon was observed owing to their limited amount and inconspicuous diffraction

intensity of graphene and carbon. Fig. 2d illustrates Raman patterns of CoS@rGO and CoS@rGO@C. Two peaks at approximate 1354 cm^{-1} and 1590 cm^{-1} of each pattern can be ascribed to disordered (D) carbon and graphitic (G) carbon structures, respectively. The intensity ratio (I_G: I_D) of the two peaks of CoS@rGO@C was 1.053, which was slightly higher than that (1.046) of CoS@rGO. This implied that the extra carbon coating on CoS@rGO@C contributed to improving the disordered carbon structure and electrical conductivity of the composite. Moreover, the contents of active CoS in both composites were also determined by TGA analysis (Fig. 2e). Specifically, the content of CoS decreased from 69.4% to 48.1% after carbon coating.

To investigate the sodium storage mechanism of the CoS@rGO@C anode, electrochemical sodiation/desodiation reaction processes were examined by cyclic voltammetry (CV) (Fig. 3a). For the initial cathodic process of CoS@rGO@C, the reduction peak at 1.2 V corresponded to the formation of Na_xCoS and the peak at 0.8 V could be assigned to the reduction reactions resulting in Na_2S and Co. Moreover, the peak at 0.55 V was ascribed to Na ion insertion into the carbon [7]. For the anodic scan, the oxidation peak at 1.8 V was ascribed to the reverse conversion reaction of Co with Na_2S. Notably, the good reproducibility of CV curves after the 1st cycle demonstrated the remarkable reversibility and stability of the electrochemical reactions of the CoS@rGO@C anode.

As shown in Fig. 3b, the initial discharge and charge capacities of CoS@rGO@C were 1018 and 706 $mAh{\cdot}g^{-1}$, respectively, and the corresponding Coulombic efficiency (CE) was 69.4%. The irreversible capacities are mainly related to the electrolyte decomposition and SEI formation on the anode surface at a voltage range between 0.08 and 0.5 V. Considering the CoS, rGO and C ingredients in CoS@rGO@C, which were 48.1%, 21.2% and 30.7%, respectively, the individual capacity contribution of CoS, rGO and C to the total capacity of CoS@rGO@C (703 $mAh{\cdot}g^{-1}$) was around 600, 42, 61 $mAh{\cdot}g^{-1}$, respectively (Fig. S1). On the second cycle, CoS@rGO@C delivered a discharge/charge capacity of 715/704 $mAh{\cdot}g^{-1}$ with a corresponding CE of 98.1%. Notably, starting from the 2nd cycle, each discharge curve possessed two similar discharge plateaus in the potential ranges of 0.98–0.9 V and 0.6–0.5 V, respectively, corresponding to the reactions of CoS and carbon with sodium. In the following charge curves, a plateau at about 1.6–1.75 V was observed, which precisely matched the abovementioned peaks on CV curves and could be attributed to the reverse electrode reaction to form CoS from Na_xCoS. One possible approach to reduce the first-cycle irreversible capacity is to presodiate the anode material. The discharge/charge voltage profiles of

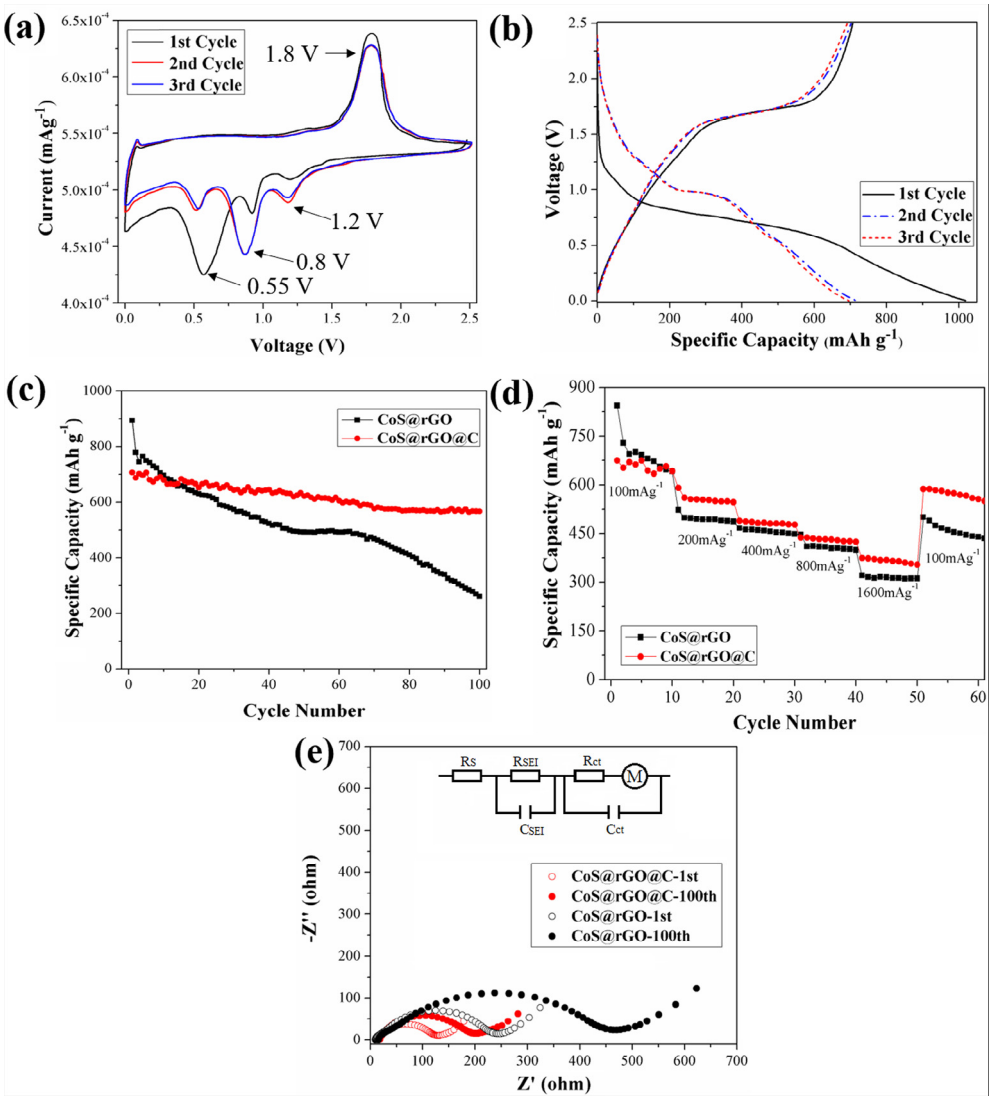

Fig. 3. (a) CV curves of CoS@rGO@C anode at a scan rate of 0.1 $mV{\cdot}s^{-1}$. (b) Galvanostatic charge–discharge curves of CoS@rGO@C anode under 0.01–2.5 V at 100 $mA{\cdot}g^{-1}$. (c) Cycling performance, (d) C-rate performance, and (e) electrochemical impedance spectra of CoS@rGO and CoS@rGO@C anodes at the 1st and 100th cycles.

CoS@rGO@C anode after presodiation are illustrated in Fig. S2. As expected, the irreversible capacity loss was effectively mitigated after presodiation, leading to an enhanced initial CE. Moreover, based on the potential plateaus appeared on the first discharge curves of bare CoS (Fig. S3) and CoS@rGO@C (Fig. 3b) anodes, the reaction mechanism of CoS against Na in our study is consistent with the previously reported two-step reaction process [7].

Supplementary data associated with this article can be found, in the online version, at https://doi.org/10.1016/j.matlet.2018.08.150.

$$CoS_2 + xNa^+ + xe^- \rightarrow Na_xCoS_2 \quad (1)$$

$$Na_xCoS_2 + (2-x)Na^+ + (2-x)e^- \rightarrow Co + Na_2S \quad (2)$$

As shown in Fig. S4, Raman spectrum also validated the recovery of CoS crystal after the first CV cycle.

Fig. 3c compares the cycling properties of CoS@rGO@C and CoS@rGO anodes at a current density of 100 $mA{\cdot}g^{-1}$. It is obvious that CoS@rGO@C showed enhanced cycling performance compared to CoS@rGO. Specifically, CoS@rGO@C retained a reversible capacity of 567 $mAh{\cdot}g^{-1}$ even after 100 cycles, whereas CoS@rGO only had 260 $mAh{\cdot}g^{-1}$ after the same cycles. Although the initial CE of CoS@rGO@C was low, it increased dramatically upon cycling, reaching over 93.5% after 5 cycles and 98.4% after 20 cycles. Fig. S5 demonstrates the SEM images of CoS@rGO (a) and CoS@rGO@C (b) after 100 cycles at a current density of 100 $mA{\cdot}g^{-1}$. It is seen that there were many obvious cracks on the surface of CoS@rGO anode after 100 cycles, which was due to the dramatic volume expansion during repeated sodiation–desodiation processes. In contrast, the CoS@rGO@C anode could effectively maintain its structural integrity and retain the sheet-like morphology of rGO. By further observing their TEM images (Fig. S6), it is found CoS clusters were better confined in CoS@rGO@C than in CoS@rGO after 100 cycles, which was due to the extra carbon coating treatment. In other words, extra carbon coating in CoS@rGO@C retarded the serious fracture of the scaffold and helped hold the active material (CoS) in the composite. Hence, the extra carbon coating is demonstrated as an effective method to accommodate the volume expansion.

Moreover, as shown in Fig. 3d, CoS@rGO@C exhibited higher rate capacities than CoS@rGO. CoS@rGO@C delivered initial reversible capacities of 675, 590, 488, and 437 $mAh{\cdot}g^{-1}$ at 100, 200, 400, and 800 $mA{\cdot}g^{-1}$, respectively. Impressively, even at a very high current rate of 1.6 $A{\cdot}g^{-1}$, CoS@rGO@C anode exhibited a reversible capacity of 374 $mAh{\cdot}g^{-1}$. Therefore, CoS@rGO@C anode exhibits high capacity performance even at very high sodium ions insertion-extraction rates.

According to the Nyquist plots shown in Fig. 3e, the impedance spectra of CoS@rGO and CoS@rGO@C anodes were composed of a semicircle at medium frequency and a sloping straight line at low frequency. From the 1st to 100th cycle, the surface layer resistances (R_s) of CoS@rGO@C and CoS@rGO increased from 9.6 to 12.3 Ω and from 13.1 to 17.6 Ω, respectively. More notably, the charge-transfer resistance (R_{ct}) of CoS@rGO@C increased from to 127 to 202 Ω during these cycles, while that of CoS@rGO increased from 224 to 466 Ω. Obviously, the better cyclic performance of CoS@rGO@C could be credited to its both lower charge transfer and surface layer resistances compared to those of CoS@rGO. In addition, the lower resistances of CoS@rGO@C might also be the probable reason for its improved rate kinetic behavior. These results implied that the presence of carbon coating on the outside of CoS@rGO composite is favorable to enhance the electronic conductivity and electrochemical performance of the electrode.

Furthermore, Table S1 compares CoS@rGO@C with previously reported cobalt sulfide-based anode materials. By comprehensively comparing the capacity, cycling stability, and applied current density, it is seen that the introduced CoS@rGO@C composite possesses comparable or higher electrochemical performance than many other cobalt sulfide-based anode materials, especially in cycling performance. It is, therefore, demonstrated that the facile carbon coating contributes greatly to the improved integrity of the composite anode during repeated cycles, thus leading to an enhanced cycle stability.

3. Conclusion

This study introduces a scalable method to fabricate CoS@rGO@C anode with superior structural integrity and highly stable electrochemical property SIBs. The extra outer carbon coating not only contributed to the electronic transfer and the volume variation accommodation, but also led to an enhanced anode performance in terms of both higher sodium ion diffusion kinetics and better cycling stability. Specifically, the CoS@rGO@C anode could maintain a reversible capacity of 567 $mAh{\cdot}g^{-1}$ up to 100 cycles at 100 $mA{\cdot}g^{-1}$. More importantly, the introduced strategy can be conveniently adapted to other metal-based anode material to improve their cycling stability in SIBs and promote their application in energy storage.

Acknowledgments

The research was funded by the Fundamental Research Funds for the Central Universities (grant number BCZD2018006) and the Special Project of International Scientific and Technological Cooperation in Guangzhou Development District (2017GH35). We also acknowledge the fund of Guangdong Province Industrial Sci. & Tech. Projects (2017A010103006) and Guangzhou Industrial Sci. & Tech. Projects (201804010368).

References

[1] Y. Ge, J. Zhu, M. Dirican, H. Jia, M. Yanilmaz, Y. Lu, C. Chen, Y.P. Qiu, X. Zhang, Fabrication and electrochemical behavior study of nano-fibrous sodium titanate composite, Mater. Lett. 188 (2017) 176–179.
[2] J. Yang, Z.L. Chen, H. Wang, F. Liang, R.S. Chen, R.B. Wu, Highly ordered three-dimensional TiO2@C nanotube arrays as freestanding electrode for sodium-ion battery, Mater. Lett. 207 (2017) 149–152.
[3] H. Jia, M. Dirican, C. Chen, J.D. Zhu, P. Zhu, C.Y. Yan, Y. Li, X. Dong, J.S. Guo, X.W. Zhang, Reduced graphene oxide-incorporated SnSb@CNF composites as anodes for high-performance sodium-ion batteries, ACS Appl. Mater. Interfaces 10 (2018) 9696–9703.
[4] H. Jia, M. Dirican, J.D. Zhu, C. Chen, C.Y. Yan, P. Zhu, Y. Li, J.S. Guo, Y. Caydamli, X. W. Zhang, High-performance SnSb@rGO@CMF composites as anode material for sodium-ion batteries through high-speed centrifugal spinning, J. Alloy. Compd. 752 (2018) 296–302.
[5] Y.C. Du, X.S. Zhu, X.S. Zhou, L.Y. Hu, Z.H. Dai, J.C. Bao, Co3S4 porous nanosheets embedded in graphene sheets as high-performance anode materials for lithium and sodium storage, J. Mater. Chem. A 3 (2015) 6787–6791.
[6] K.Y. Xie, L. Li, X. Deng, W. Zhou, Z.P. Shao, A strongly coupled CoS2/reduced graphene oxide nanostructure as an anode material for efficient sodium-ion batteries, J. Alloy. Compd. 726 (2017) 394–402.
[7] X.M. Zhu, X.Y. Jiang, X.L. Liu, L.F. Xiao, X.P. Ai, H.X. Yang, Y.L. Cao, Amorphous CoS nanoparticle/reduced graphene oxide composite as high-performance anode material for sodium-ion batteries, Ceram. Int. 43 (2017) 9630–9635.